












RESEARCH ARTICLE | MARCH 08 2024

Ground-induced suppression of chaos in the self-excited flow behind a plunging airfoil

Richard C. C. Chung; Yu Guan (关昱)  ; Wei He (何伟)  ; Wen Ao (敖文)  ; Bo Yin (尹博) ; Zhijian Yang (杨智健) ; Mohammad Hossein Doranehgard ; Larry K. B. Li  



Physics of Fluids 36, 034111 (2024)

<https://doi.org/10.1063/5.0195683>



View
Online



Export
Citation

Articles You May Be Interested In

Propulsive performance of plunging airfoils in biplane configuration

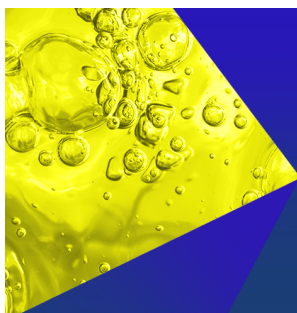
Physics of Fluids (March 2022)

On plunging using double-peak kinematics

Physics of Fluids (October 2024)

Geometric control analysis of the unsteady aerodynamics of a pitching–plunging airfoil in dynamic stall

Physics of Fluids (March 2024)



Physics of Fluids
Special Topics
Open for Submissions

[Learn More](#)

Ground-induced suppression of chaos in the self-excited flow behind a plunging airfoil

Cite as: Phys. Fluids **36**, 034111 (2024); doi: [10.1063/5.0195683](https://doi.org/10.1063/5.0195683)

Submitted: 3 January 2024 · Accepted: 19 February 2024 ·

Published Online: 8 March 2024



View Online



Export Citation



CrossMark

Richard C. C. Chung,¹ Yu Guan (关昱),^{2,a)} Wei He (何伟),^{3,a)} Wen Ao (敖文),^{4,a)} Bo Yin (尹博),¹ Zhijian Yang (杨智健),¹ Mohammad Hossein Doranehgard,¹ and Larry K. B. Li^{1,a)}

AFFILIATIONS

¹Department of Mechanical and Aerospace Engineering, The Hong Kong University of Science and Technology, Clear Water Bay, Hong Kong

²Department of Aeronautical and Aviation Engineering, The Hong Kong Polytechnic University, Kowloon, Hong Kong

³School of Science and Technology, City University of London, Northampton Square, London EC1V 0HB, United Kingdom

⁴National Key Laboratory of Solid Rocket Propulsion, Northwestern Polytechnical University, Xi'an, China

^{a)}Authors to whom correspondence should be addressed: yu.guan@polyu.edu.hk; wei.he.3@city.ac.uk; aw@nwpu.edu.cn; and larryli@ust.hk

ABSTRACT

We numerically investigate the forced synchronization of the self-excited flow behind a plunging airfoil in ground effect at a Reynolds number of $Re = 1000$. On varying the plunging amplitude and frequency, we find a rich array of nonlinear dynamics, such as a period-1 limit cycle due to natural vortex shedding as well as two-frequency quasiperiodicity on a torus attractor (T^2). For certain non-resonant plunging frequencies without a ground surface, we find that low-dimensional chaos emerges via the Ruelle–Takens–Newhouse route. However, we find that the chaos can be suppressed by introducing a ground surface, inducing a direct transition from T^2 quasiperiodicity to 1:1 phase locking as the plunging amplitude rises over the boundaries of the Arnold tongue. Apart from suppressing chaos, the ground surface also causes the lift and drag coefficients to become less sensitive to the plunging motion itself. Knowledge of the critical plunging conditions required for forced synchronization and chaos could be useful in various engineering applications, such as the design of pico air vehicles.

Published under an exclusive license by AIP Publishing. <https://doi.org/10.1063/5.0195683>

I. INTRODUCTION

In recent years, pico air vehicles (PAVs) have attracted significant interest owing to their potential to revolutionize operations such as search and rescue, surveillance and reconnaissance, robotic pollination, and environmental monitoring.¹ This is motivated by the view that such operations would benefit from enhanced coverage and increased resilience to hardware or software failure if swarms of tiny, maneuverable and possibly disposable PAVs were deployed in place of large-scale costly individual robots. PAVs are defined as uncrewed aerial machines whose maximum linear dimension is 5 cm or less and whose maximum takeoff mass is 500 mg or less.¹ These physical boundaries overlap with those of flying insects (e.g., fruit flies and bumblebees),² prompting researchers to draw inspiration from nature when designing PAVs.^{3–5}

A key challenge in designing effective PAVs is to understand and exploit the peculiar aerodynamics found at small length and velocity scales. Micro-air vehicles are the size of large birds, operating at

chord-based Reynolds numbers of $Re > 10^4$; their aerodynamics are typically dominated by turbulent flow.² Nano-air vehicles are one size class smaller, operating at $10^3 < Re < 10^4$; their aerodynamics are in the transition regime, strongly influenced by boundary layer separation and possible reattachment.¹ By contrast, PAVs operate at even lower Reynolds numbers, $Re < 3 \times 10^3$; their aerodynamics are dominated by laminar flow, implying that unsteady mechanisms can be used to increase lift above that, which could be achieved with only steady mechanisms.¹ PAVs typically operate under strict power constraints owing to their limited energy storage capabilities. Thus, it is important to develop strategies to enhance the aerodynamic performance of PAVs, with a common approach being to draw inspiration from nature.⁶ In this context, plunging airfoils are often studied to gain physical insight into the unsteady aerodynamics of natural flapping-wing flyers.^{7,8} However, only a few studies involving plunging airfoils have previously been performed at Re values low enough to be relevant to PAVs ($Re < 3 \times 10^3$), and none has considered the effect of ground

proximity, which is crucial during the takeoff and landing phases of flight.

In this numerical study, we adopt a forced synchronization framework to explore the unsteady aerodynamics of a rigid two-dimensional airfoil—with a National Advisory Committee for Aeronautics (NACA) 0012 profile—plunging sinusoidally in ground effect at conditions relevant to PAVs: a low Reynolds number ($Re = 1000$) and a moderate angle of attack ($\alpha = 10^\circ$). By systematically varying the plunging frequency (f_p) and amplitude (a) for different values of ground clearance (h), we find various nonlinear states, such as vortex shedding on a period-1 limit cycle, two-frequency quasiperiodicity on a torus attractor, low-dimensional deterministic chaos on a strange attractor, and phase locking on a period-1 orbit. By analyzing those states with tools from dynamical systems theory, we find that the chaotic state emerges via the classic torus-breakdown route, but that it can be suppressed simply by introducing a ground surface. This shows that the spectral composition and complexity of the aerodynamic force fluctuations acting on a prototypical airfoil at low Re can depend sensitively on h , with potentially wider implications for the design and optimization of future PAVs.

Before presenting our numerical setup and validation (Sec. II) and results (Sec. III), we survey the literature on the low- Re aerodynamics of stationary (Sec. IA) and plunging (Sec. IB) airfoils, both without and with the ground effect. We then review how airfoil motion can induce chaos in the wake dynamics (Sec. IC), before posing the research questions of this study (Sec. ID).

A. Stationary airfoils: Without and with ground effect

To establish a baseline, we first consider a stationary airfoil without a ground nearby. Kurtulus⁹ has numerically investigated the flow around a NACA 0012 airfoil at $0^\circ \leq \alpha \leq 90^\circ$ and $Re = 1000$. We choose to set our angle of attack at $\alpha = 10^\circ$ because Kurtulus⁹ showed that at $\alpha \geq 8^\circ$, a stationary airfoil in a steady uniform free-stream can produce vortex shedding at a well-defined natural frequency, f_n . In the flow instability literature, such periodic shedding is known as a nonlinear global mode,¹⁰ which arises from a sufficiently large region of local absolute instability.¹¹

Introducing a ground surface under a stationary airfoil can drastically alter the flow instability characteristics. For example, using numerical simulations and a bi-global stability analysis, He *et al.*¹² investigated the separated flow around a NACA 4415 airfoil in ground effect at conditions relevant to PAVs: low Reynolds numbers ($300 \leq Re \leq 1000$) and a high angle of attack ($\alpha = 20^\circ$). They found that the Kelvin–Helmholtz mode is dominant, producing a nonlinear global mode, in the form of periodic vortex shedding, via a supercritical Hopf bifurcation. They also found the time-averaged coefficients of lift ($\overline{C_l}$) and drag ($\overline{C_d}$) scale inversely with h for a moving ground, but linearly with h for a stationary ground. In all the cases examined, the flow was found to be at either a fixed point or a periodic limit cycle, with no clear evidence of more complex dynamics such as quasiperiodicity or chaos. In follow-up work, He *et al.*¹³ found for similar flow conditions that increasing h amplifies the energy gain and causes the optimal perturbations to become two dimensional. They also found that the absolute/convective instability characteristics are highly dependent on the recirculation region downstream of the airfoil.

Qu *et al.*¹⁴ numerically examined the unsteady flow around a NACA 4412 airfoil at a relatively high Reynolds number of

$Re = 3 \times 10^5$, with a focus on comparing the static ground effect (SGE) and the dynamic ground effect (DGE). Here, SGE refers to a stationary airfoil in the ground effect, whereas DGE refers to an airfoil translating toward or away from the ground. The latter case can be considered a single-plunge test case, offering insight into the aerodynamics of a plunging airfoil during its downstroke. The SGE results of Qu *et al.*¹⁴ showed that for a non-dimensional ground clearance of $H \equiv h/c < 0.1$ (where c is the chord length of the airfoil), lift is inversely proportional to H , consistent with the findings of He *et al.*¹² For DGE, the aerodynamic parameter space was found to contain three distinct regimes, delineated by two critical values of H : 0.5 and 1.0. For $H \geq 1.0$, the ground has only a minor influence on the aerodynamics and could, thus, be considered absent. However, as H decreases, lift increases similarly to that for SGE when $0.5 \leq H < 1.0$ and particularly rapidly when $H < 0.5$.¹⁴ Lift also increases with the sink velocity: when the airfoil is plunged more quickly toward the ground, the air under the airfoil has less time to escape, increasing the local static pressure and hence increasing lift.¹⁴

B. Plunging airfoils: Without and with ground effect

Numerous studies have examined plunging airfoils, but most of them have focused on relatively high Reynolds numbers of $Re \geq 10^4$. For example, Young and Lai¹⁵ numerically simulated the unsteady flow around a sinusoidally plunging NACA 0012 airfoil at $Re = 2 \times 10^4$. They found that the aerodynamic coefficients and wake patterns are sensitive to the reduced frequency of the plunging motion. At low reduced frequencies, the aerodynamic coefficients were found to be governed by leading-edge flow separation. The flow structures in the wake, however, were found to be governed by trailing-edge effects over a wide range of reduced frequencies. In follow-up work, Young and Lai¹⁶ examined a similar airfoil under similar flow conditions and found that the wake dynamics can exhibit vortex lock-in if the plunging amplitude is sufficiently high. Such synchronization behavior is analogous to that which is often observed in hydrodynamically self-excited wakes behind an oscillating cylinder.^{17,18} However, Young and Lai¹⁶ also found that the lock-in regime, known as the Arnold tongue in the synchronization literature,^{19,20} is asymmetric about $f_p/f_n = 1$. This asymmetry was attributed to the sharp trailing edge inducing flow separation on the windward side of the airfoil, particularly at high f_p .¹⁶ A similar asymmetry in the Arnold tongue was observed by Choi *et al.*²¹ in simulations performed at $Re = 300$.

In a combined experimental–numerical study at $500 \leq Re \leq 10^5$, Jones *et al.*²² examined the Knoller–Betz effect, whereby a plunging airfoil can generate thrust. For Strouhal numbers above unity, the wake structures were found to be asymmetric, producing lift and thrust on an average basis. Lai and Platzer²³ then reported on water-tunnel experiments of a plunging NACA 0012 airfoil at $500 \leq Re \leq 2.1 \times 10^4$. They found that, above a critical plunging velocity, the flow topology can change from drag to thrust producing, with the downstream wake transforming into a jet.

Turning to the ground effect, Molina and Zhang²⁴ numerically studied the aerodynamic performance of an inverted airfoil plunging sinusoidally above a ground surface at $Re = 3.9 \times 10^5$. Depending on the phase lag between the plunging motion and the aerodynamic coefficients, the flow was found to be dominated by three distinct effects. At low f_p , the airfoil motion can be treated as quasi-stationary, causing the flow to be dominated by the classic ground effect. At intermediate

f_p , the effective α becomes important, with the maximum downforce occurring at high effective α owing to the incidence effect. At high f_p , the vertical acceleration of the airfoil dominates the generation of downforce, consistent with the added mass effect.

C. Chaotization due to airfoil motion

When an airfoil oscillates under specific conditions, its wake can transition from a regular state of periodic vortex shedding to an irregular state of low-dimensional deterministic chaos via a catalog of universal routes.^{25,26} Characterizing these routes to chaos and the associated nonlinear dynamics—such as quasiperiodicity and intermittency—is important because they could hold the key to unlocking latent improvements in aerodynamic performance. Such a strategy has been demonstrated throughout aerospace engineering, particularly in the analysis of aeroelastic airfoil systems.^{27–30} Furthermore, many routes to chaos can be readily modeled and understood, implying that their characterization serves to offer deeper insights into the underlying flow physics. For example, Badrinath *et al.*³¹ numerically studied the wake dynamics of a NACA 0012 airfoil ($Re = 1000$, $\alpha = 0^\circ$) plunging sinusoidally at a fixed reduced frequency of 2. Using nonlinear time-series analysis and recurrence plots, they found that as the plunging amplitude increases, the wake can transition from periodicity to chaos via type-I intermittency. In a follow-up study, Bose and Sarkar³² numerically investigated the effect of imposing a combined pitching–plunging motion to the same airfoil (NACA 0012) at the same Reynolds number ($Re = 1000$). As the motion amplitude was increased at a fixed reduced frequency of 2, the flow was found to transition from periodic vortex shedding to chaos via quasiperiodicity, which is consistent with the torus-breakdown route to chaos.³³ This route has also been observed by Bose *et al.*³⁴ in an elastically mounted airfoil undergoing pitching–plunging motion and by Blondeaux *et al.*³⁵ in an airfoil oscillating in the hovering mode. Recently, Bose *et al.*³⁶ examined the link between wake transitions in the near- and far-fields of a pitching–plunging airfoil at low Re , revealing the key effects of aperiodic jet-switching and leading-edge vortex formation on the transition to chaos.

D. Contributions of the present study

In previous studies where low-dimensional chaos was observed in the flow around a plunging airfoil, f_p was held constant while the plunging amplitude was varied. This single-parameter variation meant that it was not possible to explore the full synchronization dynamics within and around the 1:1 Arnold tongue.^{19,20} In particular, it was not possible to identify the boundaries of the chaotic regime in the synchronization map. Crucially, those studies were performed with the airfoil in complete isolation, so a key question naturally arises: how would the presence of a ground surface under a plunging airfoil affect the transition to chaos at a Reynolds number relevant to PAVs? A second question is how would the forced synchronization dynamics change with changes in both the plunging amplitude and frequency of the airfoil, with the latter taking on values both below and above f_n itself.

II. NUMERICAL SETUP AND VALIDATION

To answer the questions posed in Sec. ID, we perform numerical simulations of the unsteady flow around a NACA 0012 airfoil plunging above a flat ground surface at an angle of attack of $\alpha = 10^\circ$ and a

Reynolds number of $Re = 1000$; here $Re \equiv U_\infty c / \nu$, where U_∞ is the free-stream velocity, c is the chord length, and ν is the kinematic viscosity. We consider these specific flow conditions because they are relevant to PAVs during takeoff and landing.¹ The trailing edge of the airfoil is at a vertical distance of h above the ground (see Fig. 1), implying a non-dimensional ground clearance of $H \equiv h/c$. We use a Cartesian coordinate system whose origin is at the quarter-chord point on the airfoil; the x coordinate is in the streamwise direction, and the y coordinate is in the transverse direction. We enable the airfoil to undergo a sinusoidal plunging motion at a non-dimensional frequency of $F \equiv f_p/f_n$, where f_p is the plunging frequency and f_n is the natural frequency of the self-excited wake, i.e., the nonlinear global mode.¹⁰ The plunging amplitude is defined non-dimensionally as $A \equiv a/c$.

The flow is governed by the incompressible continuity and Navier–Stokes equations,

$$\nabla \cdot \vec{V} = 0, \quad (1)$$

$$\frac{\partial \vec{V}}{\partial t} + (\vec{V} \cdot \nabla) \vec{V} = -\frac{1}{\rho} \nabla p + \nu \nabla^2 \vec{V}, \quad (2)$$

where \vec{V} , p , and ρ are the flow velocity, pressure, and density, respectively. Equations (1) and (2) are solved numerically in two dimensions using OpenFOAM, an open-source code based on the finite volume method. Pressure–velocity coupling is applied with the pressure-implicit with the splitting of operators (PISO) algorithm. Five corrector steps are used, with time steps ranging from 10^{-4} to 10^{-3} . For cases with airfoil motion, the solver is combined with dynamic mesh computations, pimpleDyMFOam. This involves computing the y -component of the velocity at each mesh point via the velocityComponentLaplacian algorithm. Table I summarizes the solver settings, and Table II lists the boundary conditions. In this study, the initial conditions are kept constant, so the basins of attraction are not mapped. Furthermore, while the injection of random perturbations in nonlinear dynamical systems is known to produce various noise-induced dynamics (e.g., coherence resonance^{37,38} and noise-induced intermittency³⁹), this is not the focus of the present study and is left for future work.

Two different types of computational mesh are used: (i: Fig. 2) Mesh-G features a slip ground surface, and (ii: Fig. 3) Mesh-NG features no ground surface at all. Both meshes are built with Gmsh,⁴⁰ an open-source mesh generator. The boundary layer around the airfoil is

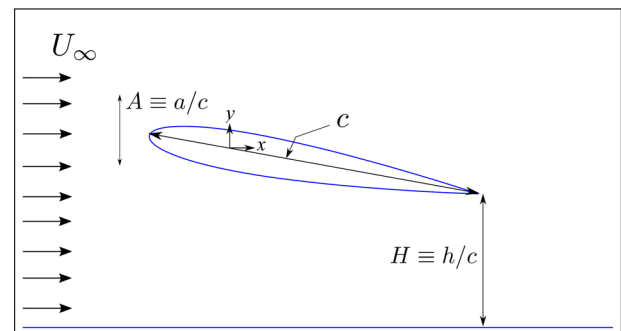


FIG. 1. Geometry of a symmetric airfoil plunging above a flat ground surface. The non-dimensional ground clearance is $H \equiv h/c$, and the non-dimensional plunging amplitude is $A \equiv a/c$.

TABLE I. Summary of OpenFOAM settings.

Discretization	
Momentum	Second-order upwind
Pressure	Second-order
Time	Second-order fully implicit
Time step	5×10^{-4}
Total simulation time	400
Segregated solver	
Non-plunging cases	icoFoam
Plunging cases	pimpleDyMFoam
Viscous model	Laminar
$p-\vec{V}$ coupling	PISO

TABLE II. Boundary conditions, where ZG denotes a zero-gradient Neumann condition.

Variables	Inlet	Outlet	Top	Ground	Airfoil
p	ZG	0	0	ZG	ZG
U_∞	1	ZG	ZG	Slip	No slip

TABLE III. Mesh properties for different values of H . For all meshes, the streamwise length of the domain is $54c$.

$H \equiv h/c$	Type	Domain height	Cell count
0.1	Mesh-G	$16.1c$	24 017
0.2	Mesh-G	$16.3c$	40 628
0.4	Mesh-G	$16.5c$	42 589
0.6	Mesh-G	$16.7c$	44 485
0.8	Mesh-G	$16.9c$	46 365
1.0	Mesh-G	$17.1c$	49 181
2.0	Mesh-G	$18.1c$	59 377
∞	Mesh-NG	$32.0c$	46 398

resolved with 50 layers of structured cells spread over a total height of $0.1c$. There is also a small region of structured cells behind the trailing edge of the airfoil. The rest of the domain consists of unstructured cells generated by the Delaunay algorithm in Gmsh. Table III lists the mesh properties for different values of H .

We validate our numerical framework against published data by examining $\overline{C_l}$, $\overline{C_d}$, and the Strouhal number St of the C_l oscillations. We consider two representative configurations: (Table IV: NACA 0012) a stationary airfoil without the ground effect⁹ and (Table V:

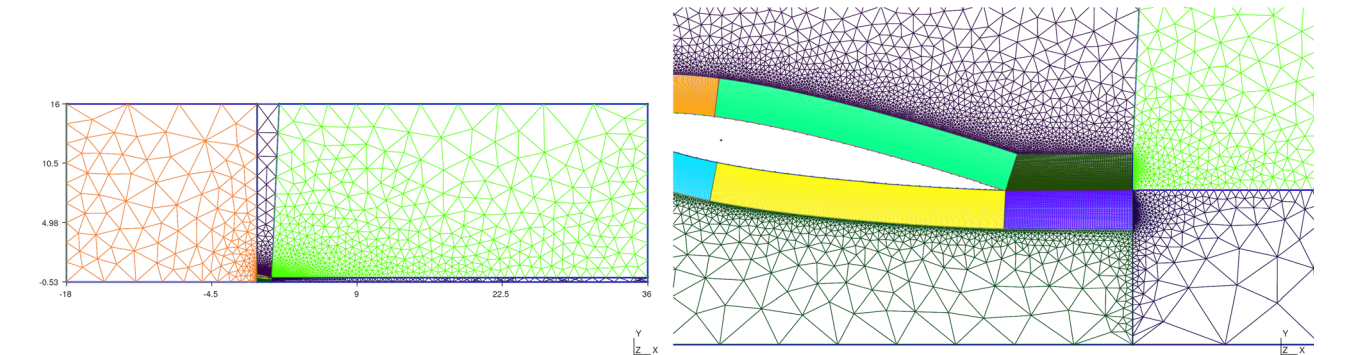


FIG. 2. Mesh-G with a ground surface: (left) overview of the computational domain, and (right) magnified view of the trailing edge of the airfoil. In this example, the non-dimensional ground clearance is $H = 0.4$.

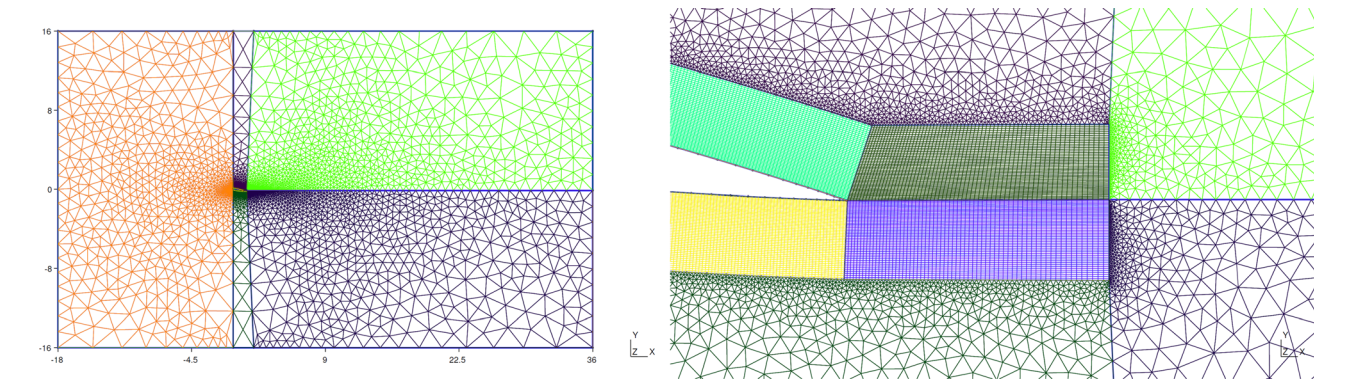


FIG. 3. Mesh-NG with no ground surface ($H = \infty$): (left) overview of the computational domain, and (right) magnified view of the trailing edge of the airfoil.

TABLE IV. Numerical validation against the data of Kurtulus⁹ for a stationary NACA 0012 airfoil without the ground effect at $Re = 1000$ and $\alpha = 10^\circ$.

	$\overline{C_l}$	$\overline{C_d}$	St
Kurtulus ⁹	0.418	0.165	0.876
Present study	0.409 61	0.163 35	0.872 17
ε_{rel}	2.00%	1.00%	0.44%

TABLE V. Numerical validation against the data of He *et al.*¹² for a stationary NACA 4415 airfoil in the ground effect ($H = 0.8$) at $Re = 500$ and $\alpha = 20^\circ$.

	$\overline{C_l}$	$\overline{C_d}$	St
He <i>et al.</i> ¹²	0.464 85	0.171 55	0.862 50
Present study	0.461 98	0.170 63	0.862 39
ε_{rel}	0.62%	0.54%	0.01%

NACA 4415) a stationary airfoil in the ground effect.¹² For both configurations, we find that the relative errors (ε_{rel}) for $\overline{C_l}$, $\overline{C_d}$, and St are all within 2%, demonstrating the accuracy of our numerical framework.

III. RESULTS AND DISCUSSION

A. A stationary airfoil in ground effect

Figure 4(a) shows the time-averaged lift and drag coefficients, $\overline{C_l}$ and $\overline{C_d}$, for the stationary airfoil at different values of H . We find an inverse relationship between both of these aerodynamic coefficients and H , with $\overline{C_l}$ increasing more markedly than $\overline{C_d}$ as H decreases. The increases in $\overline{C_l}$ and $\overline{C_d}$ are gradual when the airfoil is far from the ground ($H > 1.0$) but become more pronounced as the airfoil approaches the ground. These observations are consistent with previous studies,^{12,24} providing further credence to our numerical framework.

Figure 4(a) also shows the Strouhal number St as a function of H . Here, $St \equiv f_n c / U_\infty$, where f_n is found by computing the power spectral density (PSD) of the C_l fluctuation signal, as shown in Fig. 4(c).

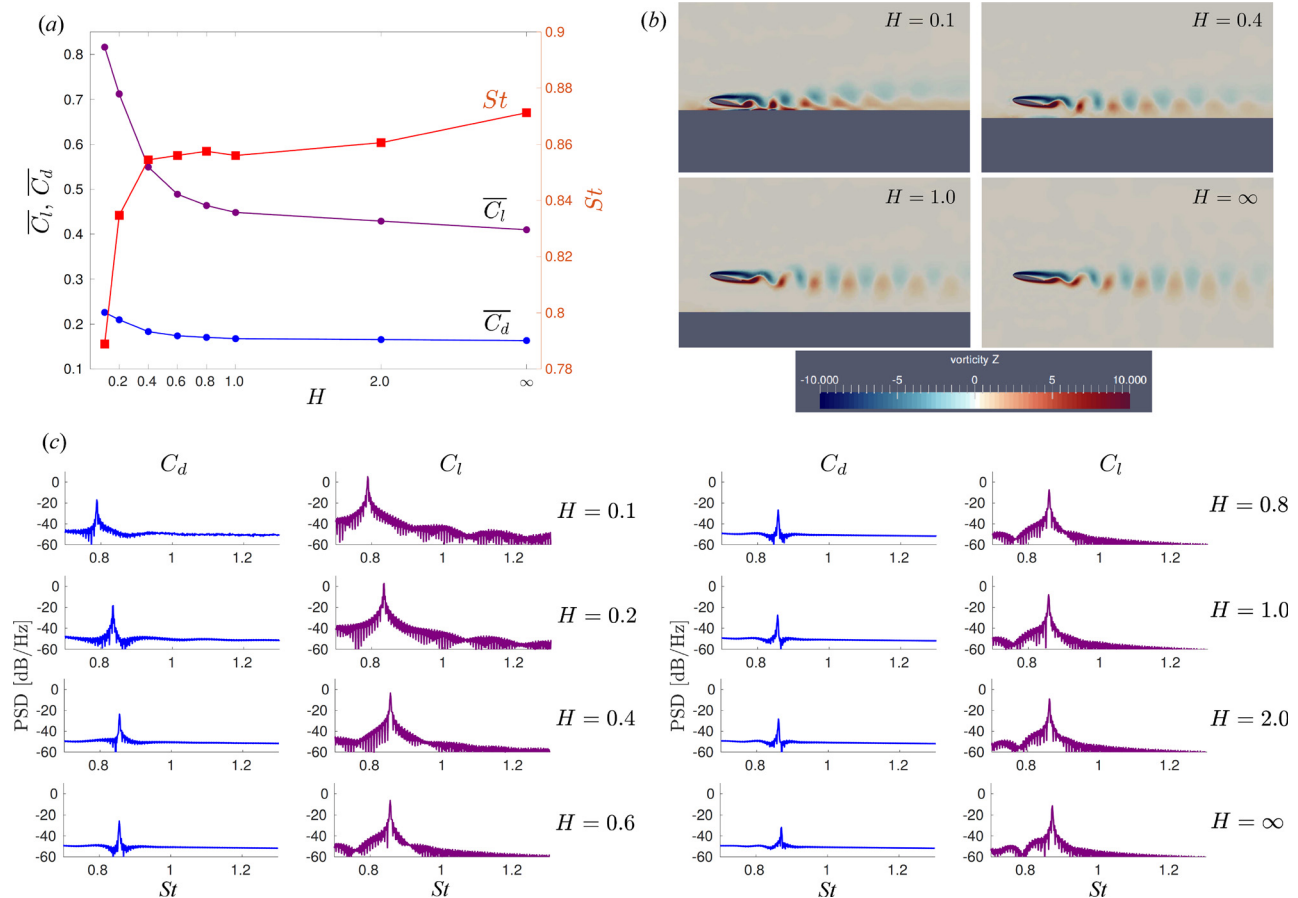


FIG. 4. Stationary airfoil in the ground effect: (a) time-averaged lift and drag coefficients and the Strouhal number, (b) instantaneous vorticity field at $t = 400$ s, and (c) PSD of the C_d and C_l fluctuation signals. Data are shown at different values of ground clearance $H \equiv h/c$. In subfigure (b), the colorbar in the top-left panel is applicable to all four panels.

We find that like $\overline{C_l}$ and $\overline{C_d}$, St varies most markedly when $H < 0.5$. However, unlike both of those aerodynamic coefficients, St decreases as the airfoil approaches the ground. For all values of H , both the C_l and C_d signals show sharp dominant peaks in their PSDs, indicating the presence of large-scale coherent flow oscillations associated with a self-excited nonlinear global mode. In other words, the system evolves on a period-1 limit-cycle attractor in phase space, as will be explored later.

To examine the nonlinear global mode of the wake, we show in Fig. 4(b) the spatial distribution of instantaneous vorticity at four values of ground clearance: $H = 0.1, 0.4, 1.0$, and ∞ . For all values of H , we find that coherent vortical structures are shed periodically from the airfoil but then dissipate as they are advected downstream. For $H = 0.1$ and 0.4 , the close proximity of the ground distorts the vortical structures, even as they are being shed, causing them to dissipate more rapidly downstream.

In summary, we have shown that introducing a ground surface under a stationary airfoil at low Re can increase both $\overline{C_l}$ and $\overline{C_d}$ but decrease St . These changes are associated with distorted vortical structures undergoing enhanced dissipation with downstream evolution. Regardless of H , we find that the wake dynamics remains dominated by a nonlinear global mode that oscillates at a discrete natural frequency. This is the classic behavior of a self-excited hydrodynamic oscillator evolving on a limit-cycle attractor in phase space.¹⁰

B. A plunging airfoil in ground effect

Next, we apply concepts from forced synchronization theory¹⁹ to understand how the self-excited flow system in Sec. III A responds to external perturbations in the form of periodic plunging of the airfoil.

1. Forced synchronization and chaos

Figure 5 shows the forced synchronization maps for three representative values of ground clearance: $H = 0.1, 0.4$, and ∞ . These maps consolidate the various states of the system in a parameter space defined by A and F .

When the ground is absent (Fig. 5: $H = \infty$), we find evidence of three dynamical states arising from airfoil motion ($A > 0$). For weak plunging at a non-resonant frequency ($F \neq 1$), the system transitions from its original self-excited state on a limit-cycle attractor (Sec. III A) to a two-frequency quasiperiodic state on a torus attractor via a Neimark–Sacker bifurcation, i.e., a secondary Hopf bifurcation.^{20,41}

The emergence of this quasiperiodic state, which is indicated by green square markers in the synchronization map (Fig. 5), is confirmed by applying nonlinear time-series analysis.⁴² Specifically, Fig. 6 shows the time trace of C_b , its PSD, its phase lag relative to the plunging motion ($\Delta\psi_{A(t),C_l}$), and its reconstructed phase space in terms of both the phase portrait and the Poincaré map (single or double sided). To reconstruct the phase space, we feed the C_l signal into the embedding algorithm of Takens,⁴³ with the optimal values of the embedding delay time (τ) and the embedding dimension (d) found via, respectively, the average mutual information function⁴⁴ and the technique proposed by Cao.⁴⁵ The phase lag $\Delta\psi_{A(t),C_l}$ is of interest as previous work has shown that flapping flyers tend to optimize their aerodynamic performance by adjusting the phase dynamics of their wing geometry.⁴⁶ The data in Fig. 6 are for a fixed plunging frequency ($F = 1.1$) but with increasing A . For comparison, we also show data for a stationary airfoil (Sec. III A). As expected for a period-1 limit-cycle attractor (Fig. 6: $A = 0$), we find a periodic time trace, a line-dominated PSD, unbounded phase evolution ($-\psi_{C_l}$), a closed orbit in the phase portrait, and a single cluster of trajectory intercepts in the single-sided Poincaré map. However, for weak plunging (Fig. 6: $A = 0.001$ and 0.004), the C_l signal develops spectral components at both f_p and f_n , along with their linear combinations. The phase lag $\Delta\psi_{A(t),C_l}$ decreases unboundedly in time, indicating phase drifting, a signature feature of quasiperiodicity.^{47,48} The reconstructed phase space shows classic evidence of a two-dimensional torus attractor (\mathbb{T}^2): a pair of closed rings in the double-sided Poincaré map.⁴² Collectively, these observations confirm that the C_l dynamics are, indeed, quasiperiodic. The plunging motion of the airfoil is simply not yet strong enough to synchronize the natural self-excited oscillations of the global hydrodynamic mode.

As A increases (still for $H = \infty$), the system transitions from \mathbb{T}^2 quasiperiodicity to one of two possible states, depending on the value of F . For most values of F , the system transitions to 1:1 phase locking

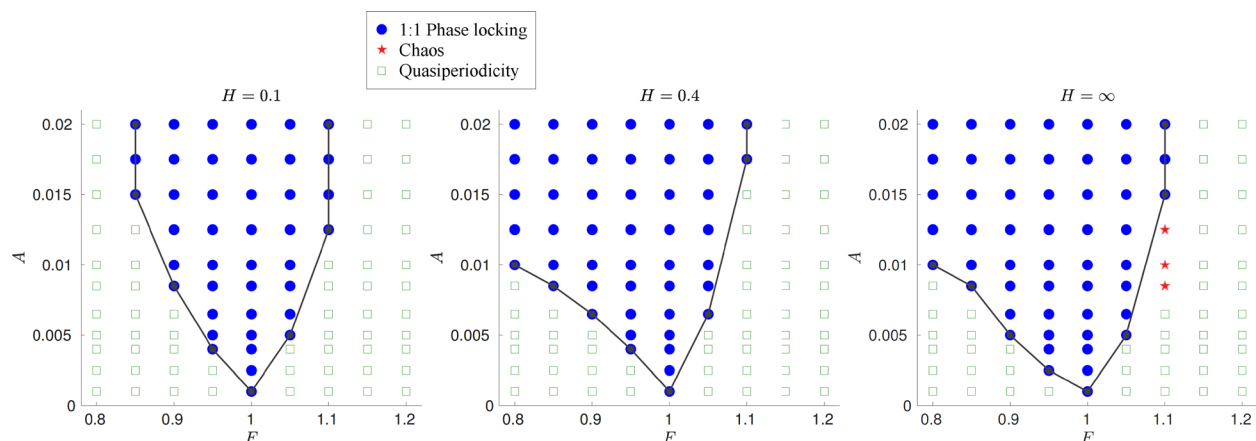


FIG. 5. Forced synchronization maps for a plunging airfoil with and without the ground effect: $H = 0.1, 0.4$, and ∞ . The parameter space is defined by $A \equiv a/c$ and $F \equiv f_p/f_n$.

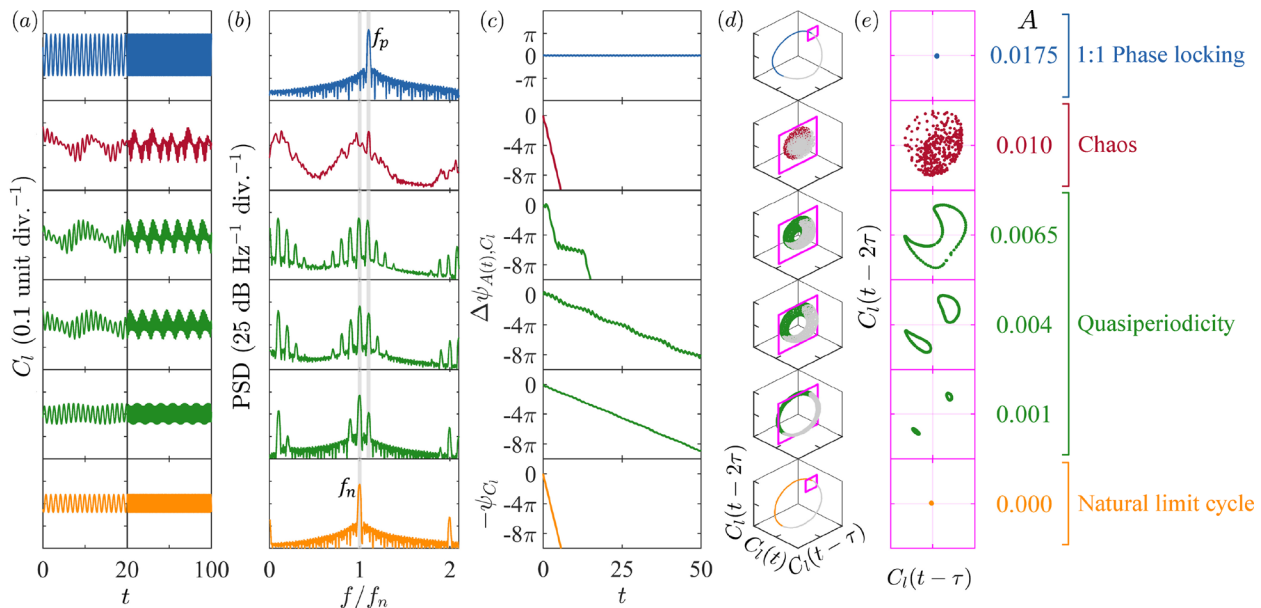


FIG. 6. Plunging airfoil without ground effect ($H = \infty$): (a) time trace of C_i , (b) its PSD, (c) its phase lag relative to the plunging motion (except for $A = 0$, where it is simply the phase evolution of the system, $-\psi_{C_i}$), and its reconstructed phase space in terms of (d) the phase portrait and (e) the Poincaré map. The single-sided or double-sided nature of the Poincaré map is indicated by the square cross section outlined in magenta in column (d). The data shown are for a fixed plunging frequency ($F = 1.1$), with A increasing from 0 to 0.0175.

on a period-1 orbit, which is a fully synchronous state represented by blue circular markers in the synchronization map (Fig. 5). We find that phase locking occurs most easily (i.e., at lower A) when the airfoil is plunging at a frequency near the natural global frequency of the flow, i.e., when F is near 1. Thus, the shape of this synchronous regime is approximately triangular, with a bottom vertex centered at $F = 1$ (Fig. 5). This synchronous regime is known as the Arnold tongue in the synchronization literature¹⁹ and has been observed before in various self-excited flow systems, such as gaseous jets^{49–51} and thermoacoustic oscillators.^{48,52} For $F = 1.1$, however, the system transitions to an intermediate state of chaos before phase locking, as represented by red star markers in the synchronization map (Fig. 5). In this chaotic regime (Fig. 6), the time trace of C_i shows irregular aperiodic fluctuations, the PSD contains energetic broadband components, and the reconstructed phase space hosts a non-smooth fractal object. These observations are consistent with the emergence of a chaotic state associated with a strange attractor.⁴² Crucially, the chaotic state emerges from the collapse of the torus attractor identified earlier (Fig. 6), indicating that it arises via the Ruelle–Takens–Newhouse route.⁵³ This is a classic route to chaos in nonlinear dynamical systems;³³ it involves the breakdown of an unstable 3-torus into a chaotic attractor via folding and stretching processes.⁵³ Nevertheless, as A increases further, the chaotic dynamics is eventually destroyed via forced synchronization, leaving behind a periodic state of 1:1 phase locking, similar to that observed at other F values where chaos is absent.

To quantify the topological self-similarity of the chaotic attractor identified earlier, we compute the correlation dimension (D_c) from the C_i signal using the algorithm of Grassberger and Procaccia.⁵⁴ The underlying assumption of this algorithm is that the probability that two points on an attractor are within a distance R of each other is

approximately equal to the probability that those two points are contained within the same R -sized cell.³³ The algorithm has been demonstrated on various physical systems, including those in aerodynamics³⁴ and thermoacoustics.^{55,56} In Figs. 7(a1), 7(b1), and 7(c), the local slope of the correlation sum is plotted against the normalized hypersphere radius (R/R_{max}) for embedding dimensions ranging from $d = 2$ to 12. For the phase-locked state [Fig. 7(a1)], we find that the data converge to a correlation dimension of $D_c \approx 1.0$. This confirms that the topological structure of the attractor is a one-dimensional orbit associated with a limit cycle. For the chaotic state [Fig. 7(b1)], we find that the correlation dimension is not an integer, $D_c \approx 2.3$, indicating the presence of strangeness in the chaotic attractor.³³ Furthermore, the fact that the value of D_c is small shows that the observed chaos is low dimensional.⁴² For the quasiperiodic state [Fig. 7(c)], we find that $D_c \approx 2.0$, confirming that the torus attractor is two dimensional, dominated by the interactions between the plunging motion of the airfoil and the natural global mode of the flow.

To further confirm the presence of deterministic chaos, we compute the permutation spectrum⁵⁷ using the C_i signal. First, we consider the counterexample of a phase-locked state (see Fig. 6: $A = 0.0175$): we find that the permutation spectra of different data subsets are well aligned with one another [Fig. 7(a2)], generating a near-zero standard deviation ζ for almost all ordinal patterns [Fig. 7(a3)]. These characteristics are consistent with a periodic attractor.^{55,57,58} For the strange attractor (see Fig. 6: $A = 0.010$), we find that the permutation spectra of different data subsets are no longer aligned with one another [Fig. 7(b2)], causing ζ to rise significantly above zero for most ordinal patterns [Fig. 7(b3)]. At the same time, we find three zero-valued ζ points associated with three forbidden patterns [inset of Fig. 7(b3): 14, 17, and 22], whose symbolic sequences are, respectively, “3142,”

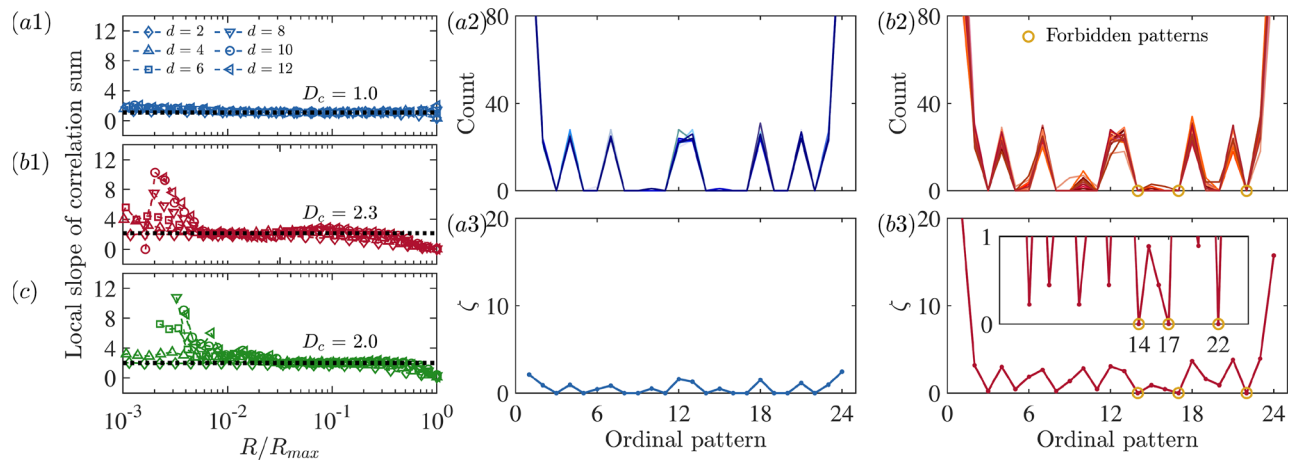


FIG. 7. [(a1), (b1), and (c)] Local slope of the correlation sum, [(a2) and (b2)] permutation spectra, and [(a3) and (b3)] their standard deviation for a plunging airfoil without the ground effect: $F = 1.1$ and $H = \infty$. The phase-locked state ($A = 0.0175$) is shown in panels (a1)–(a3), the chaotic state ($A = 0.010$) is shown in panels (b1)–(b3), and the quasiperiodic state ($A = 0.004$) is shown in panel (c). The correlation sum is computed with a delay time of $\tau = 0.12$ s. The permutation spectra are computed with an embedding dimension of $d = 4$ and $\tau = 0.12$ s using 20 different subsets of a time series with 10 000 data points (duration of 100 s).

“3412,” and “4231” as per Parlitz *et al.*⁵⁹ These permutation spectrum tests provide further evidence of deterministic chaos in the strange attractor.⁵⁷

When a ground surface is introduced (Fig. 5: $H = 0.1$ and 0.4), we find that the observed chaos disappears. As A increases at a fixed $F \neq 1$, the system transitions first (i) from its original limit-cycle state (Sec. III A) to a two-frequency quasiperiodic state via a Neimark-Sacker bifurcation, and subsequently (ii) to a synchronous state of 1:1 phase locking. This sequence of transitions is similar to that observed in the absence of a ground ($H = \infty$), with the key difference being that there is no longer any evidence of chaos between the quasiperiodic and phase-locked states. In other words, the introduction of a ground surface has suppressed chaos at the boundary between quasiperiodicity and phase locking.

Other notable differences in the synchronization dynamics arising from the introduction of a ground surface include a tilting of the Arnold tongue toward low plunging frequencies when the airfoil is moderately close to the ground (Fig. 5: $H = 0.4$), such that phase locking is more easily attained when $F < 1$ than when $F > 1$. However, when the airfoil is exceedingly close to the ground (Fig. 5: $H = 0.1$), the observed asymmetry in the Arnold tongue weakens, with phase locking occurring at similar values of A on both sides of $F = 1$.

To examine the flow topology corresponding to the three different states (quasiperiodicity, chaos and phase locking), we show in Fig. 8 the instantaneous velocity field around the airfoil when plunging at $A = 0.0125$ and $F = 1.1$ for three different values of ground clearance: $H = 0.1, 0.4$, and ∞ . For all three states, we find large-scale vortex shedding behind the airfoil, producing an alternating sequence of coherent vortical structures, which are reminiscent of those seen in the nonlinear global mode behind the stationary airfoil [Fig. 4(b)]. As was the case for the stationary airfoil, we find that as H decreases, the ground enhances the circulation of the vortices, inhibiting their dissipation and enabling them to persist farther downstream. The flow structures for $H = \infty$ are the least periodic and the most diffused, consistent with this being a chaotic state.

2. Effect of A and F on the lift and drag coefficients

Figure 9 shows colormaps of $\overline{C_l}$ and $\overline{C_d}$ in the same A - F parameter space used in Fig. 5. Here, both $\overline{C_l}$ and $\overline{C_d}$ have been normalized by their unforced values to highlight their relative changes and are denoted by η_l and η_d , respectively. As in Fig. 5, three representative values of ground clearance are considered: $H = 0.1, 0.4$, and ∞ . In each

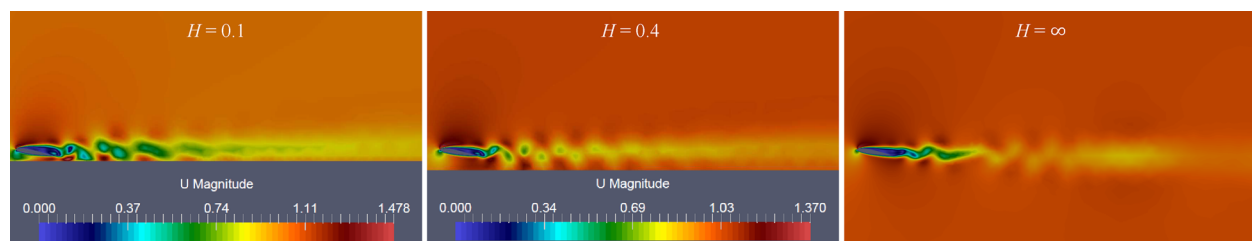


FIG. 8. Instantaneous velocity field around a plunging airfoil with and without the ground effect: (left) $H = 0.1$, phase locking; (middle) $H = 0.4$, quasiperiodicity; and (right) $H = \infty$, chaos. In all cases, $A = 0.0125$ and $F = 1.1$. The colorbar for $H = \infty$ is the same as that for $H = 0.4$. For clarity, only a partial region of the full computational domain is shown.

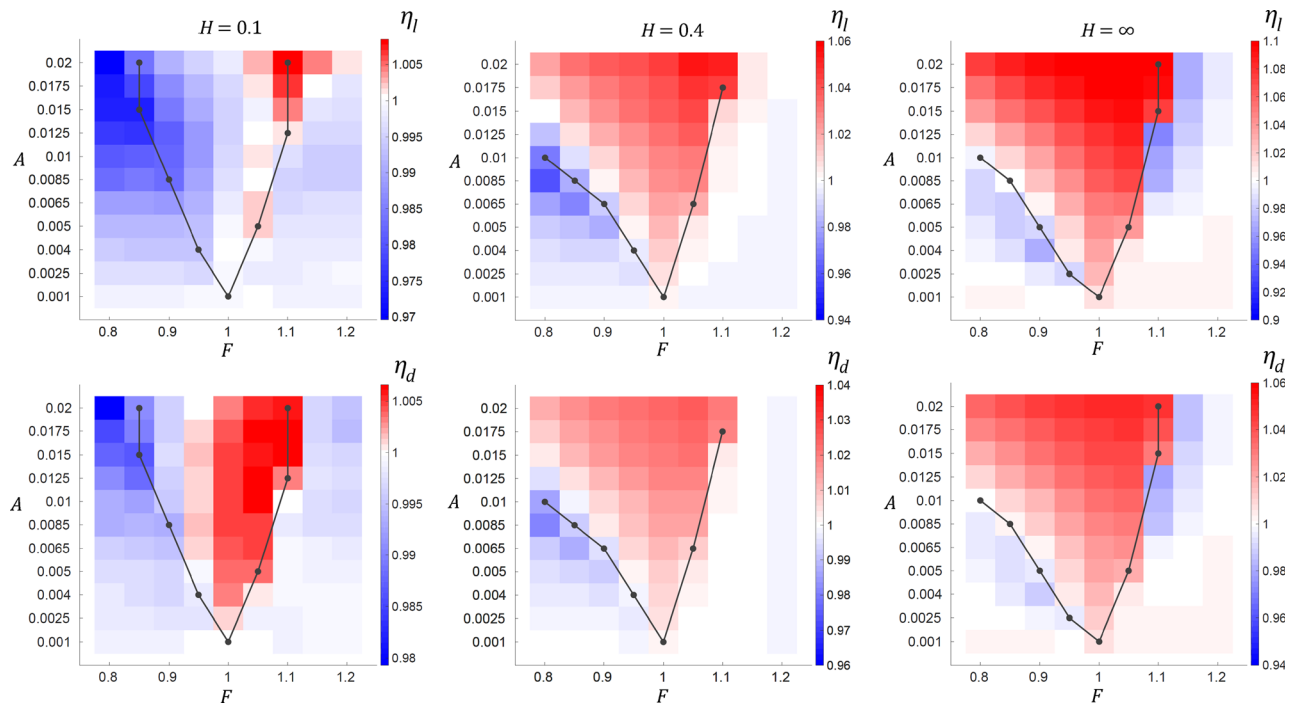


FIG. 9. Aerodynamic coefficients of a plunging airfoil with and without the ground effect (left to right: $H = 0.1, 0.4, \infty$): (top row) normalized lift coefficient η_l and (bottom row) normalized drag coefficient η_d . The parameter space is defined by $A \equiv a/c$ and $F \equiv f_p/f_n$. The black lines indicate the lower boundaries of the Arnold tongue, as identified in Fig. 5.

case, the lower boundaries of the Arnold tongue, as identified in Fig. 5, are overlaid as black lines.

When the ground is absent (Fig. 9: $H = \infty$), we find that both η_l and η_d are highest within the Arnold tongue at $F > 1$. The highest values of η_l and η_d are slightly but consistently greater than unity, indicating that plunging the airfoil at an amplitude high enough to induce phase locking can increase both $\overline{C_l}$ and $\overline{C_d}$ relative to a stationary airfoil. However, when the plunging motion changes such that the system transitions out of phase locking and into quasiperiodicity or chaos (i.e., moving just below the Arnold tongue), both η_l and η_d drop markedly, sometimes to values below unity. Thus, $\overline{C_l}$ and $\overline{C_d}$ can increase or decrease relative to the stationary airfoil case, depending on the degree of forced synchronization achieved by the plunging motion.

As the airfoil approaches the ground (Fig. 9: $H = 0.1$ and 0.4), we find that the ranges in which η_l and η_d vary become narrower, with both their maximum and minimum values moving closer to unity. Specifically, when H decreases from ∞ to 0.1 , the maximum deviations of η_l and η_d from unity decrease from 10% to 3% and from 6% to 2%, respectively. This demonstrates that as the airfoil approaches the ground, both its lift and drag coefficients become less sensitive to the plunging motion.

IV. CONCLUSIONS

We have numerically investigated the forced synchronization of the self-excited flow behind a prototypical rigid airfoil (NACA 0012) plunging sinusoidally in time. The unique features of this study are that the Reynolds number ($Re = 1000$) is low enough to be relevant to PAVs, and that the effect of a ground surface is

explicitly explored for such low- Re conditions for the first time. By systematically varying A and F for different values of ground clearance (H), we found various nonlinear states, beginning with a period-1 limit cycle associated with natural self-excited vortex shedding—a nonlinear global mode—when the airfoil was stationary ($A = 0$). On increasing A at a non-resonant F , we found the emergence of quasiperiodic dynamics on a two-dimensional torus attractor (\mathbb{T}^2) via a Neimark–Sacker bifurcation. In the absence of a ground surface ($H = \infty$), we found that further increases in A can give rise to low-dimensional deterministic chaos via the Ruelle–Takens–Newhouse route. However, we also found that the chaos can be suppressed simply by introducing a ground surface, leading to a direct transition from \mathbb{T}^2 quasiperiodicity to 1:1 phase locking as A increases at the boundaries of the Arnold tongue. In addition to suppressing chaos, the ground surface also made the lift and drag coefficients less sensitive to the plunging motion of the airfoil. By applying concepts from nonlinear dynamics and synchronization, this study has provided an improved understanding of the unsteady aerodynamics of an airfoil plunging in ground effect at low Re . This could facilitate the design and optimization of PAVs for various applications, such as emergency rescue and environmental monitoring. Future research directions include investigating the effects of a combined plunging–pitching motion,³² a movable leading edge,⁶⁰ and a non-flat ground surface.⁶¹ Other potential areas of research include incorporating the effects of random perturbations and gusts^{62,63} as well as mapping the basins of attraction by systematically varying the initial conditions.⁶⁴

ACKNOWLEDGMENTS

This work was supported by the Research Grants Council of Hong Kong (Project Nos. 16210419 and 16200220). Y.G. was supported by the PolyU Start-up Fund (Project No. P0043562).

AUTHOR DECLARATIONS

Conflict of Interest

The authors have no conflicts to disclose.

Author Contributions

Richard C. C. Chung: Data curation (equal); Investigation (equal); Writing – original draft (equal). **Yu Guan:** Investigation (equal); Writing – review & editing (equal). **Wei He:** Formal analysis (equal); Investigation (equal); Methodology (equal); Supervision (equal); Writing – review & editing (equal). **Wen Ao:** Investigation (equal); Writing – review & editing (equal). **Bo Yin:** Investigation (equal); Writing – review & editing (equal). **Zhijian Yang:** Investigation (equal); Writing – review & editing (equal). **Mohammad Hossein Doranehgard:** Investigation (equal); Writing – review & editing (equal). **Larry K. B. Li:** Conceptualization (equal); Investigation (equal); Project administration (equal); Supervision (equal); Writing – original draft (equal); Writing – review & editing (equal).

DATA AVAILABILITY

The data that support the findings of this study are available from the corresponding authors upon reasonable request.

REFERENCES

- ¹R. J. Wood, B. Finio, M. Karpelson, K. Ma, N. O. Pérez-Arancibia, P. S. Sreetharan, H. Tanaka, and J. P. Whitney, “Progress on ‘pico’ air vehicles,” *Int. J. Rob. Res.* **31**, 1292–1302 (2012).
- ²R. Dudley, *The Biomechanics of Insect Flight: Form, Function, Evolution* (Princeton University Press, 2002).
- ³K. D. Jones, C. J. Bradshaw, J. Papadopoulos, and M. F. Platzer, “Bio-inspired design of flapping-wing micro air vehicles,” *Aeronaut. J.* **109**, 385–393 (2005).
- ⁴H. Liu, S. Ravi, D. Kolomenskiy, and H. Tanaka, “Biomechanics and biomimetics in insect-inspired flight systems,” *Philos. Trans. R. Soc. B* **371**, 20150390 (2016).
- ⁵Y. Bao, H. Ping, H. Zhu, D. Zhou, Y. Yang, and Z. Han, “Laminar wake suppression of airfoil by rotating rod at low Reynolds number,” *Phys. Rev. Fluids* **7**, 034102 (2022).
- ⁶M. H. Dickinson, C. T. Farley, R. J. Full, M. A. R. Koehl, R. Kram, and S. Lehman, “How animals move: An integrative view,” *Science* **288**, 100–106 (2000).
- ⁷T. J. Mueller, *Fixed and Flapping Wing Aerodynamics for Micro Air Vehicle Applications* (American Institute of Aeronautics and Astronautics, 2001).
- ⁸W. Shyy, Y. Lian, J. Tang, H. Liu, P. Trizila, B. Stanford, L. Bernal, C. Cesnik, P. Friedmann, and P. Ifju, “Computational aerodynamics of low Reynolds number plunging, pitching and flexible wings for MAV applications,” *Acta Mech. Sin.* **24**, 351–373 (2008).
- ⁹D. F. Kurtulus, “On the unsteady behavior of the flow around NACA 0012 airfoil with steady external conditions at $Re = 1000$,” *Int. J. Micro Air Veh.* **7**, 301–326 (2015).
- ¹⁰P. Huerre and P. A. Monkewitz, “Local and global instabilities in spatially developing flows,” *Annu. Rev. Fluid Mech.* **22**, 473–537 (1990).
- ¹¹J. M. Chomaz, P. Huerre, and L. G. Redekopp, “Bifurcations to local and global modes in spatially developing flows,” *Phys. Rev. Lett.* **60**, 25–28 (1988).
- ¹²W. He, P. Yu, and L. K. B. Li, “Ground effects on the stability of separated flow around a NACA 4415 airfoil at low Reynolds numbers,” *Aerosp. Sci. Technol.* **72**, 63–76 (2018).
- ¹³W. He, J. M. Pérez, P. Yu, and L. K. B. Li, “Non-modal stability analysis of low-Re separated flow around a NACA 4415 airfoil in ground effect,” *Aerosp. Sci. Technol.* **92**, 269–279 (2019).
- ¹⁴Q. Qu, X. Jia, W. Wang, P. Liu, and R. K. Agarwal, “Numerical study of the aerodynamics of a NACA 4412 airfoil in dynamic ground effect,” *Aerosp. Sci. Technol.* **38**, 56–63 (2014).
- ¹⁵J. Young and C. S. J. Lai, “Oscillation frequency and amplitude effects on the wake of a plunging airfoil,” *AIAA J.* **42**, 2042–2052 (2004).
- ¹⁶J. Young and C. S. J. Lai, “Vortex lock-in phenomenon in the wake of a plunging airfoil,” *AIAA J.* **45**, 485–490 (2007).
- ¹⁷G. H. Koopmann, “The vortex wakes of vibrating cylinders at low Reynolds numbers,” *J. Fluid Mech.* **28**, 501–512 (1967).
- ¹⁸M. Provansal, C. Mathis, and L. Boyer, “Bénard-von Kármán instability: Transient and forced regimes,” *J. Fluid Mech.* **182**, 1–22 (1987).
- ¹⁹A. S. Pikovsky, M. G. Rosenblum, and J. Kurths, *Synchronization: A Universal Concept in Nonlinear Sciences*, Cambridge Nonlinear Science Series (Cambridge University Press, Cambridge, England, 2003).
- ²⁰A. Balanov, N. Janson, D. Postnov, and O. Sosnovtseva, *Synchronization: From Simple to Complex* (Springer-Verlag, Heidelberg, Germany, 2009).
- ²¹J. Choi, T. Colonius, and D. R. Williams, “Surging and plunging oscillations of an airfoil at low Reynolds number,” *J. Fluid Mech.* **763**, 237–253 (2015).
- ²²K. D. Jones, C. M. Dohring, and M. F. Platzer, “Experimental and computational investigation of the Knoller–Betz effect,” *AIAA J.* **36**, 1240–1246 (1998).
- ²³C. S. J. Lai and M. F. Platzer, “Jet characteristics of a plunging airfoil,” *AIAA J.* **37**, 1529–1537 (1999).
- ²⁴J. Molina and X. Zhang, “Aerodynamics of a heaving airfoil in ground effect,” *AIAA J.* **49**, 1168–1179 (2011).
- ²⁵D. Lentink and M. Gerritsma, “Influence of airfoil shape on performance in insect flight,” AIAA Paper No. 2003-3447, 2003.
- ²⁶D. Lentink, F. T. Muijres, F. J. Donker-Duyvis, and J. L. Van Leeuwen, “Vortex-wake interactions of a flapping foil that models animal swimming and flight,” *J. Exp. Biol.* **211**, 267–273 (2008).
- ²⁷Q. Liu, Y. Xu, and J. Kurths, “Active vibration suppression of a novel airfoil model with fractional order viscoelastic constitutive relationship,” *J. Sound Vib.* **432**, 50–64 (2018).
- ²⁸Q. Liu, Y. Xu, J. Kurths, and X. Liu, “Complex nonlinear dynamics and vibration suppression of conceptual airfoil models: A state-of-the-art overview,” *Chaos* **32**, 062101 (2022).
- ²⁹W. Guo, Y. Xu, Y. Li, Q. Liu, and X. Liu, “Dynamic responses of a conceptual two-dimensional airfoil in hypersonic flows with random perturbations,” *J. Fluids Struct.* **121**, 103920 (2023).
- ³⁰Q. Liu, Y. Xu, and Y. Li, “Complex dynamics of a conceptual airfoil structure with consideration of extreme flight conditions,” *Nonlinear Dyn.* **111**, 14991–15010 (2023).
- ³¹S. Badrinath, C. Bose, and S. Sarkar, “Identifying the route to chaos in the flow past a flapping airfoil,” *Eur. J. Mech. B* **66**, 38–59 (2017).
- ³²C. Bose and S. Sarkar, “Investigating chaotic wake dynamics past a flapping airfoil and the role of vortex interactions behind the chaotic transition,” *Phys. Fluids* **30**, 047101 (2018).
- ³³R. C. Hilborn, *Chaos and Nonlinear Dynamics* (Oxford University Press, 2000).
- ³⁴C. Bose, S. Gupta, and S. Sarkar, “Transition to chaos in the flow-induced vibration of a pitching-plunging airfoil at low Reynolds numbers: Ruelle–Takens–Newhouse scenario,” *Int. J. Non Linear Mech.* **109**, 189–203 (2019).
- ³⁵P. Blondeaux, L. Guglielmini, and M. S. Triantafyllou, “Chaotic flow generated by an oscillating foil,” *AIAA J.* **43**, 918–921 (2005).
- ³⁶C. Bose, S. Gupta, and S. Sarkar, “Dynamic interlinking between near- and far-field wakes behind a pitching-heaving airfoil,” *J. Fluid Mech.* **911**, A31 (2021).
- ³⁷Y. Zhu, V. Gupta, and L. K. B. Li, “Coherence resonance in low-density jets,” *J. Fluid Mech.* **881**, R1 (2019).
- ³⁸M. Lee, Y. Zhu, L. K. B. Li, and V. Gupta, “System identification of a low-density jet via its noise-induced dynamics,” *J. Fluid Mech.* **862**, 200–215 (2019).
- ³⁹H. S. Varun, M. S. Aswathy, and S. Sarkar, “A complex networks based approach to nonlinear aeroelasticity,” *J. Fluids Struct.* **121**, 103912 (2023).
- ⁴⁰C. Geuzaine and J. F. Remacle, “Gmsh: A 3-D finite element mesh generator with built-in pre- and post-processing facilities,” *Numer. Methods Eng.* **79**, 1309–1331 (2009).

- ⁴¹M. Murugesan, Y. Zhu, and L. K. B. Li, "Complex network analysis of forced synchronization in a hydrodynamically self-excited jet," *Int. J. Heat Fluid Flow* **76**, 14–25 (2019).
- ⁴²H. Kantz and T. Schreiber, *Nonlinear Time Series Analysis*, 2nd ed. (Cambridge University Press, Cambridge, England, 2003).
- ⁴³F. Takens, "Detecting strange attractors in turbulence," in *Dynamical Systems and Turbulence*, Lecture Notes in Mathematics Vol. 898, edited by D. Rand and L. Young (Springer-Verlag, New York, 1981), pp. 366–381.
- ⁴⁴A. M. Fraser and H. L. Swinney, "Independent coordinates for strange attractors from mutual information," *Phys. Rev. A* **33**, 1134 (1986).
- ⁴⁵L. Cao, "Practical method for determining the minimum embedding dimension of a scalar time series," *Physica D* **110**, 43–50 (1997).
- ⁴⁶S. Ramanarivo, R. Godoy-Diana, and B. Thiria, "Rather than resonance, flapping wing flyers may play on aerodynamics to improve performance," *Proc. Natl. Acad. Sci. U. S. A.* **108**, 5964–5969 (2011).
- ⁴⁷L. K. B. Li and M. P. Juniper, "Phase trapping and slipping in a forced hydrodynamically self-excited jet," *J. Fluid Mech.* **735**, R5 (2013).
- ⁴⁸Y. Guan, V. Gupta, M. Wan, and L. K. B. Li, "Forced synchronization of quasiperiodic oscillations in a thermoacoustic system," *J. Fluid Mech.* **879**, 390–421 (2019).
- ⁴⁹L. K. B. Li and M. P. Juniper, "Lock-in and quasiperiodicity in hydrodynamically self-excited flames: Experiments and modelling," *Proc. Combust. Inst.* **34**, 947–954 (2013).
- ⁵⁰L. K. B. Li and M. P. Juniper, "Lock-in and quasiperiodicity in a forced hydrodynamically self-excited jet," *J. Fluid Mech.* **726**, 624–655 (2013).
- ⁵¹A. K. Kushwaha, N. A. Worth, J. R. Dawson, V. Gupta, and L. K. B. Li, "Asynchronous and synchronous quenching of a globally unstable jet via axisymmetry breaking," *J. Fluid Mech.* **937**, A40 (2022).
- ⁵²Y. Guan, V. Gupta, K. Kashinath, and L. K. B. Li, "Open-loop control of periodic thermoacoustic oscillations: Experiments and low-order modelling in a synchronization framework," *Proc. Combust. Inst.* **37**, 5315–5323 (2019).
- ⁵³S. Newhouse, D. Ruelle, and F. Takens, "Occurrence of strange Axiom A attractors near quasiperiodic flows on T^m , $m \geq 3$," *Commun. Math. Phys.* **64**, 35–40 (1978).
- ⁵⁴P. Grassberger and I. Procaccia, "Characterization of strange attractors," *Phys. Rev. Lett.* **50**, 346 (1983).
- ⁵⁵Y. Guan, M. Murugesan, and L. K. B. Li, "Strange nonchaotic and chaotic attractors in a self-excited thermoacoustic oscillator subjected to external periodic forcing," *Chaos* **28**, 093109 (2018).
- ⁵⁶Y. Guan, L. K. B. Li, B. Ahn, and K. T. Kim, "Chaos, synchronization, and desynchronization in a liquid-fueled diffusion-flame combustor with an intrinsic hydrodynamic mode," *Chaos* **29**, 053124 (2019).
- ⁵⁷C. W. Kulp and L. Zunino, "Discriminating chaotic and stochastic dynamics through the permutation spectrum test," *Chaos* **24**, 033116 (2014).
- ⁵⁸Y. Guan, V. Gupta, and L. K. B. Li, "Intermittency route to self-excited chaotic thermoacoustic oscillations," *J. Fluid Mech.* **894**, R3 (2020).
- ⁵⁹U. Parlitz, S. Berg, S. Luther, A. Schirdewan, J. Kurths, and N. Wessel, "Classifying cardiac biosignals using ordinal pattern statistics and symbolic dynamics," *Comput. Biol. Med.* **42**, 319–327 (2012).
- ⁶⁰E. A. R. Camacho, M. M. da Silva, A. R. R. Silva, and F. D. Marques, "Real-time optimization of wing drag and lift performance using a movable leading edge," *Phys. Fluids* **36**, 016128 (2024).
- ⁶¹W. He, Y. Guan, V. Theofilis, and L. K. B. Li, "Stability of low-Reynolds-number separated flow around an airfoil near a wavy ground," *AIAA J.* **57**, 29–34 (2019).
- ⁶²H. Jiang, "Exact momentum sources for gust injection in flow simulations," *Phys. Fluids* **35**, 096115 (2023).
- ⁶³K. Panta, H. Deng, B. Cheng, and A. Panah, "Navigating vortex gust interactions and mitigations by plunging wings," *Phys. Fluids* **36**, 011901 (2024).
- ⁶⁴E. Ott, *Chaos in Dynamical Systems*, 2nd ed. (Cambridge University Press, Cambridge, UK, 2002).